Generalized numerical renormalization-group method to calculate the thermodynamical properties of impurities in metals

Wanda C. Oliveira* and Luiz N. Oliveira
Departamento de Física e Ciência dos Materiais, Instituto de Física e Química de São Carlos, Universidade de São Paulo, 13560-970 São Carlos, SP, Brazil
(Received 14 December 1993)

A dimensionless discretization parameter Λ controls the accuracy and the computational cost of numerical renormalization-group calculations. For reliable computations of thermodynamical properties of impurities in metals, the upper bound $\Lambda \leq 3$ has long been established. This report discusses a generalization that raises the limit to $\Lambda = 10$, yielding the same accuracy with significantly smaller computational cost.

I. INTRODUCTION

This paper discusses an extension of the numerical renormalization-group approach to the calculation of thermodynamical properties of impurities in metals. For the computation of a given property, compared to the original method,[1] the generalized approach yields the same accuracy with substantially smaller numerical effort. It therefore overcomes an obstacle that has restricted applications of the method.

The numerical renormalization-group approach was developed to compute the contribution of impurities to the thermodynamical properties of metals. Two early applications calculated the temperature-dependent magnetic susceptibility for the Kondo and Anderson models for dilute magnetic alloys.[1,2] More recent examples are the computations of the low-temperature magnetic susceptibility and specific heat for the two-impurity Kondo model.[3,4]

The procedure is founded upon a logarithmic discretization of the conduction band. A dimensionless parameter $\Lambda > 1$, the ratio between two successive discrete energies, controls this approximation and defines the cost of a given computation. For $\Lambda \to 1$, the conduction-band continuum being recovered, the procedure would become exact. In that limit, however, the cost of calculating the partition function for any given Hamiltonian would be infinite. Practical values of Λ are therefore significantly larger than unity. They are chosen by weighing the computational cost, which decreases exponentially with $1/\ln\Lambda$, against the accuracy with which physical properties can be computed, which deteriorates in the same proportion.

Wilson[1] has presented analytical arguments indicating that computed thermodynamical averages depend very weakly on the discretization parameter Λ, so that averages computed with $\Lambda \lesssim 3$ should be within a few percent of the exact limit. The numerical computations of the impurity magnetic susceptibility $\chi_{\rm imp}$ as a function of the temperature T for the Kondo[1] and Anderson[2] models, carried out for various discretization parameters in the interval $2 \leq \Lambda \leq 3$, have confirmed that analysis. Since then, the upper limit, $\Lambda = 3$, has become the standard for calculations of $\chi_{\rm imp}(T)$.

With $\Lambda = 3$, the diagonalization of a spin-degenerate single-impurity Hamiltonian is inexpensive. Unfortunately, the computational effort increases exponentially with the degeneracy of the conduction states and with the number of impurities. This rapid growth offers a practical limitation that obstructs applications of the method. In particular, the computation of the specific heat and magnetic susceptibility in the recent numerical renormalization-group study of the two-impurity model[3–5] had to focus only on the low-temperature fixed points. The cost of diagonalizing many-impurity Hamiltonians, even spin-degenerate ones, is prohibitive. Due to the same limitation, few full-scale renormalization-group computations of thermodynamical properties have been reported.[2,6–9]

A generalized renormalization-group procedure—one based on a modified discretization of the conduction band—has been described by Yoshida *et al.*[10] That extension was developed to compute excitation properties of impurity models and has been tested in a number of golden-rule computations.[10–13] Such studies indicate that the results depend so weakly on the discretization parameter Λ that transition rates calculated with $\Lambda = 10$ deviate negligibly from the continuum limit.

In this paper, we adapt the generalized renormalization-group procedure to the computation of thermodynamical properties. To distinguish the new averaging method from the standard one, we refer to it as the *interleaved* method, a nomenclature justified in Sec. V. We discuss the Λ-dependent deviations of the calculated averages from the continuum limit and show that for given Λ, compared with the standard procedure, the interleaved procedure yields considerably smaller deviations; averages within a few percent of the continuum limit can be obtained with $\Lambda = 10$.

Although most of our discussion is concentrated on an illustrative example—the magnetic susceptibility for the single-impurity $U = 0$ Anderson Hamiltonian—the new method is equally efficient for more complex models. To show this, in an introductory overview of the

procedure we present the magnetic susceptibility for the single-impurity, spin-degenerate Kondo model calculated by the interleaved method with $\Lambda = 10$—a computation carried out in a small fraction of the time required by the standard method with $\Lambda = 3$—and show that, on the scale of the plot, its temperature dependence cannot be distinguished from the exact universal curve.[14] By combining satisfactory accuracy with relatively small computational effort, the interleaved procedure broadens the scope of the renormalization-group approach; it should, for instance, make accessible to modest computational budgets the temperature-dependent impurity susceptibility for the two-impurity Kondo or Anderson model.

Our development occupies four sections. Section II presents the preliminary overview of the interleaved procedure, comparing its results to those of the standard method. A more systematic description of the new method appears in Secs. III and IV, the former reviewing the generalized renormalization-group procedure, and the latter explaining how it can be applied to the computation of thermodynamical averages. As an illustration, Sec. V then shows that the magnetic susceptibility for the $U = 0$ Anderson model computed with $\Lambda = 10$ agrees very well with results obtained with much smaller discretization parameters. Conclusions are summarized in Sec. VI.

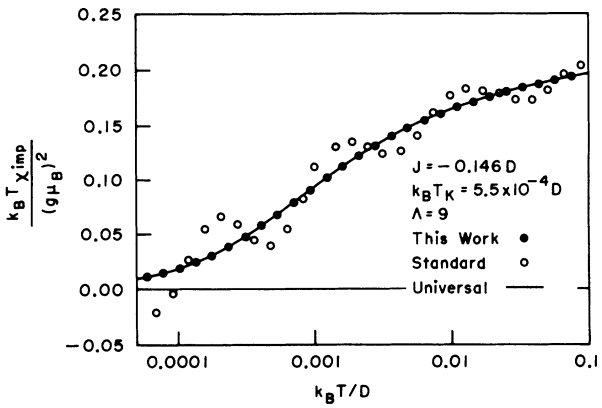

FIG. 1. Numerical renormalization-group results for the temperature dependence of the impurity magnetic susceptibility for the Kondo Hamiltonian with impurity–conduction-band coupling $J = -0.146D$. The open circles represent the thermodynamical average calculated with the standard procedure (Ref. 1) and $\Lambda = 9$. As discussed in the text, the oscillation is an artifact of the discretization whose amplitude increases rapidly with Λ. Similar oscillations appear for any single choice of z. By contrast, the generalized procedure described in this paper yields the monotonous curve represented by solid circles. For comparison, a solid line shows the universal curve computed by the Bethe ansatz.

II. OVERVIEW

The computation of the magnetic susceptibility for the Kondo model has been discussed by Wilson.[1] The model Hamiltonian, comprising conduction states $c_{k\mu}$ interacting antiferromagnetically with a localized magnetic impurity described by spin-1/2 variable $\mathbf{S}$, is

$$H = H_{cb} - J\sum_{k,k'} c^{\dagger}_{k\mu}\sigma_{\mu\nu}c_{k'\nu}\cdot\mathbf{S}, \tag{1}$$

where H_{cb} is the conduction-band Hamiltonian, which will be discussed in further detail in Sec. III. Results for the impurity contribution to the susceptibility ($\chi_{\rm imp}$) calculated with discretization parameter $\Lambda = 9$ by the standard method are shown as open circles in Fig. 1. For comparison, a solid line shows the universal curve for the susceptibility, calculated by the Bethe ansatz.[14] For such a large discretization parameter, the calculated susceptibility oscillates markedly around the exact result.

That the oscillation is an artifact of the discretization is readily recognized, for (i) its period is $\ln\Lambda$ and (ii) its amplitude grows rapidly with Λ: When the open circles in the figure are recalculated with different discretization parameters, for diminishing Λ one finds results rapidly convergent to the continuum limit. For $\Lambda = 3$, for instance, the amplitude of the oscillations is smaller by a factor of 100, so that on the scale of the plot the calculated points would be indistinguishable from the solid line. It is for this reason that calculations of thermodynamical averages have hitherto been restricted to discretization parameters $\Lambda \leq 3$.

By contrast, the susceptibility calculated with the interleaved procedure, shown by solid circles in Fig. 1, shows no oscillations; the calculated susceptibility converges much more rapidly to the continuum limit, so that even with $\Lambda = 9$ the computed curve virtually coincides with the continuum limit. As a consequence, the new procedure makes it possible to compute thermodynamical averages with large Λ, resulting in substantial savings in the computational effort. The modifications of the numerical renormalization-group method responsible for this achievement are described in Secs. III and IV.

III. GENERALIZED NUMERICAL RENORMALIZATION-GROUP METHOD

Since the generalized renormalization-group transformation procedure upon which our method is founded has been detailed in previous publications,[10,15] only brief discussion seems called for here. As in the standard numerical renormalization-group method,[2] the generalized transformation applies to model Hamiltonians of the form

$$H = H_{\rm imp} + H_{cb} + H_{\rm int}, \tag{2}$$

where $H_{\rm imp}$ is the impurity Hamiltonian, H_{cb} describes a half-filled structureless band of width $2D$ containing noninteracting electrons, and $H_{\rm int}$ is the interaction between the conduction and impurity electrons. It is based on a logarithmic discretization of the conduction band, a controllable approximation affecting only H_{cb}; both $H_{\rm imp}$ and $H_{\rm int}$ are treated exactly.

The novel ingredient in the procedure detailed by Yoshida *et al.*[10] is the pattern in Fig. 2, a generalization of the standard discretization grid.[2] The extended

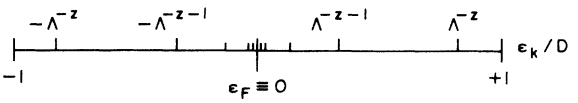

FIG. 2. Logarithmic discretization of the conduction band. Two parameters define the sequence of intervals marked by ticks below the horizontal axis: Λ must be larger than unity and z must be in the interval $0 < z \leq 1$; otherwise the two numbers are arbitrary.

procedure involves two discretization parameters Λ and z. The former, introduced by Wilson, can in principle be any number larger than unity; the latter, which we shall refer to as the *sliding* parameter, is arbitrary in the interval $0 < z \leq 1$. With $z = 1$, the standard discretization is recovered.

Figure 2 divides the positive conduction band energies ϵ_k into an infinite sequence of intervals of the form $D > \epsilon_k \geq D\Lambda^{-z}$, $D\Lambda^{-z} > \epsilon_k \geq D\Lambda^{-z-1}, \ldots, D\Lambda^{1-z-m} > \epsilon_k \geq D\Lambda^{-z-m}, \ldots$. A sequence of negative energies is likewise defined. For each positive (negative) interval, we then define a Fermionic operator a_{m+} (a_{m-}) as the most localized conduction state centered at the impurity site that can be constructed out of the energies in it. Thus, for the leading intervals in the two sequences, we define the operators

$$a_{\pm} = \pm[D(1-\Lambda^{-z})]^{-1/2} \int_{\pm D\Lambda^{-z}}^{\pm D} c_k \, d\epsilon_k, \tag{3}$$

and for the mth subsequent interval, the operators

$$a_{m\pm} = \pm [D(1-\Lambda^{-1})]^{-1/2} \Lambda^{(m+z-1)/2} \times \int_{\pm D\Lambda^{-z-m}}^{\pm D\Lambda^{1-z-m}} c_k \, d\epsilon_k. \tag{4}$$

The central approximation in the method then consists of projecting the conduction Hamiltonian

$$H_{cb} = \int_{-D}^{D} \epsilon_k c_k^{\dagger} c_k \, d\epsilon_k, \tag{5}$$

on the basis of the operators $\{a_{\pm}, a_{m\pm}\}$ ($m = 1, 2, \ldots, \infty$), i.e., of writing

$$H_{cb} = E_0(z,\Lambda)(a_+^{\dagger} a_+ - a_-^{\dagger} a_-) + \sum_{m=1}^{\infty} \left[E_m(z,\Lambda)(a_{m+}^{\dagger} a_{m+} - a_{m-}^{\dagger} a_{m-}) \right], \tag{6}$$

where

$$E_0(z,\Lambda) = \int_{D\Lambda^{-z}}^{D} \epsilon_k \, d\epsilon_k \Big/ \int_{D\Lambda^{-z}}^{D} d\epsilon_k \tag{7}$$

and

$$E_m(z,\Lambda) = \int_{D\Lambda^{-z-m}}^{D\Lambda^{1-z-m}} \epsilon_k \, d\epsilon_k \Big/ \int_{D\Lambda^{-z-m}}^{D\Lambda^{1-z-m}} d\epsilon_k \tag{8}$$

are the average energies in each of the intervals in Fig. 2. For given z and Λ, these energies constitute a discrete set. As z varies from zero to unity, they sweep over all energies in the continuum of the conduction Hamiltonian, Eq. (5).

The projection of the conduction-band Hamiltonian on the (incomplete) discrete basis is an approximation controlled by Λ. For $\Lambda \to 1$ the continuum of the conduction band is recovered, but that limit is clearly beyond the reach of numerical computations. Thus, the diagonalization of the model Hamiltonian has to be carried out with $\Lambda > 1$ and the convergence of the calculated physical properties to the continuum must be demonstrated *a posteriori*.

For numerical applications, the infinite series on the right-hand side of Eq. (6) must be truncated. The truncation, a somewhat elaborate procedure, will be discussed below; here, we observe that this second approximation, involving only the discretized conduction operators, does not affect the impurity Hamiltonian $H_{\rm imp}$. In order to ensure that it does not affect the coupling $H_{\rm int}$ between the impurity and the conduction band either, we must now give attention to $H_{\rm int}$. To be definite, we shall assume that the impurity interacts only with electrons in the Wannier state

$$f_0 = \frac{1}{\sqrt{2}} \sum_k c_k, \tag{9}$$

centered at the impurity site.

The latter is a linear combination of the $\{a_{\pm}, a_{m\pm}\}$ ($m = 1, 2, \ldots, \infty$) conduction states defined in Eqs. (3) and (4),

$$f_0 = \sqrt{\frac{1-\Lambda^{-z}}{2}}(a_+ + a_-) + \sqrt{\frac{1-\Lambda^{-1}}{2}} \sum_{m=1}^{\infty} \left[\Lambda^{(1-z-m)/2}(a_{m+} + a_{m-}) \right]. \tag{10}$$

Before diagonalizing the model Hamiltonian, accordingly, we define a new discrete basis $\{f_n\}$ ($n = 0, 1, \ldots, \infty$) by the Lanczos construction[16] starting with the Wannier state f_0. This casts the conduction-band Hamiltonian into the codiagonal form

$$H_{cb} = \sum_{n=0}^{\infty} \epsilon_n^z (f_n^{\dagger} f_{n+1} + \text{H.c.}), \tag{11}$$

with coefficients ϵ_n^z given by the recursive equation[10]

$$\prod_{n=0}^{N} (\epsilon_n^z)^2 = F_N(z,\Lambda) - \left[(\mathcal{H}_{N+1})^{2N+2} \right]_{11}, \tag{12}$$

where

$$F_N(z,\Lambda) = (1-\Lambda^{-z}) \left[E_0(z,\Lambda) \right]^{2N+2} + (1-\Lambda^{-1}) \sum_{m=1}^{\infty} \Lambda^{1-z-m} \left[E_m(z,\Lambda) \right]^{2N+2}, \tag{13}$$

$\mathcal{H}$ is the $(N+1) \times (N+1)$ matrix whose elements are

$$[\mathcal{H}_{N+1}]_{ij} = \epsilon^z_{i-1}\delta_{i,j-1} + \epsilon^z_{j-1}\delta_{j,i-1}, \quad i,j = 1,2,\ldots,N+1, \quad (14)$$

and E_0 and E_m ($m = 1,2,\ldots$) are given by Eqs. (7) and (8).

For $N = 0$, the second term on the right-hand side of Eq. (12) vanishes, so that ϵ^z_0 can be easily determined. The matriz $\mathcal{H}_{11}$ can then be constructed, following which Eq. (12) with $N = 1$ becomes an explicit expression for ϵ_1. Successive recursions determine $\epsilon_2,\epsilon_3,\ldots$. For sufficiently large N, the coefficients ϵ_n ($n \geq N$) are described to several decimal places by the approximate expression[10]

$$\epsilon^z_n = \frac{1+\Lambda^{-1}}{2} v_F \Lambda^{1-z-n/2}, \quad (15)$$

where v_F is the Fermi velocity. Just how large N must be to make this expression correct to a given accuracy depends on Λ, but for practical purposes, $N = 10$ is typically sufficient to guarantee four or more accurate significant digits in Eq. (15).

Once the ϵ^z_n have been determined, Eq. (11) describes the conduction band, while the impurity Hamiltonian $H_{\rm imp}$ and the interaction term $H_{\rm int}$ are written in their original forms, which involve only the impurity degrees of freedom and the conduction operator f_0. Still, the model Hamiltonian $H = H_{\rm imp} + H_{\rm int} + H_{cb}$ cannot be diagonalized numerically, for the series on the right-hand side of Eq. (11) is infinite; at this point, therefore, one must specify the energy scale(s) defined by the physical properties to be computed: In particular, in a calculation of thermodynamical properties at the temperature T, the energy scale of interest is $\epsilon_T = k_B T$. Energies significantly smaller than ϵ_T in the model Hamiltonian can be disregarded. Thus, if one chooses an integer L such that

$$\epsilon^z_L \ll k_B T \quad (16)$$

or, more quantitatively,

$$\epsilon^z_L = \overline{\beta} k_B T, \quad (17)$$

where $\overline{\beta}$ is small, the infinite sum on the right-hand side of Eq. (11) can be truncated at L, and the conduction-band Hamiltonian written in the approximate form

$$H_{cb} = \sum_{n=0}^{L-1} \epsilon^z_n (f^\dagger_n f_{n+1} + \text{H.c.}). \quad (18)$$

With this, the conduction-band Hamiltonian has been projected on a finite basis, and the model Hamiltonian can be diagonalized numerically. To define a renormalization-group transformation, the model Hamiltonian must next be scaled. To this effect, it is multiplied by $2\Lambda^{(L-1)/2+z-1}/[v_F(1+\Lambda^{-1})]$, a factor chosen so that the smallest codiagonal energy on the right-hand side of Eq. (18), ϵ^z_{L-1}, scales to unity [cf. Eq.(15)]. One thus defines the scaling factor

$$D_L = \frac{(1+\Lambda^{-1})v_F}{2} \Lambda^{-(L-1)/2-z+1}, \quad (19)$$

the scaled Hamiltonian

$$H_L = \left[\sum_{n=0}^{L-1} \epsilon^z_n (f^\dagger_n f_{n+1} + \text{H.c.}) + H_{\rm imp} + H_{\rm int} \right] \Big/ D_L, \quad (20)$$

and the renormalization-group transformation $\mathcal{T}$ by the relation

$$H_{L+1} \equiv \mathcal{T}[H_L]. \quad (21)$$

Physically, the transformation amounts to examining the physical properties of the model system with finer resolution, at an energy scale reduced by $\Lambda^{1/2}$. To do this, one must augment the truncated series within brackets on the right-hand side of Eq. (20); i.e., one must let $L \to L+1$. The factor multiplying the square brackets is at the same time magnified by $\sqrt{\Lambda}$, which is equivalent to choosing a smaller energy unit in which to express the Hamiltonian; this recurrent scaling makes the smallest energies in the conduction-band Hamiltonian H_{cb} of the order of unity. Since H_{cb} has no characteristic energy scale, its eigenvalues remain invariant under such a scaling; by contrast the impurity and interaction Hamiltonians normally have characteristic energies that are substantially changed under the renormalization-group transformation. This constitutes the basis for the concepts of fixed-point and crossover Hamiltonians.[1,6,15]

IV. $U = 0$ ANDERSON HAMILTONIAN

As an illustration, we now consider the Anderson model for $U = 0$. In this case, the impurity Hamiltonian simply associates an energy ϵ_d with each electron at the impurity site,

$$H_{\rm imp} = \epsilon_d c^\dagger_d c_d, \quad (22)$$

while the interaction Hamiltonian couples the impurity level c_d to the conduction levels c_k:

$$H_{\rm int} = \sqrt{2} V (c^\dagger_d f_0 + \text{H.c.}), \quad (23)$$

where f_0 was defined in Eq. (9). Spin sums are implicit in Eqs. (22) and (23). The conduction band is defined as in Sec. III, and we consider the linear dispersion relation

$$\epsilon_k = D \frac{k}{k_F}, \quad (24)$$

where k_F is the Fermi momentum, equal to unity in appropriately chosen units, and the conduction energies ϵ_k and momenta k are measured from the Fermi level and the Fermi momentum, respectively. The truncated, scaled, discretized model Hamiltonian then takes the form

$$H_L = \left[\sum_{n=0}^{L-1} \epsilon^z_n (f^\dagger_n f_{n+1} + \text{H.c.}) + \epsilon_d c^\dagger_d c_d + \sqrt{2} V (c^\dagger_d f_0 + \text{H.c.}) \right] \Big/ D_L. \quad (25)$$

This quadratic Hamiltonian can be written as the matrix product

$$H_L = \mathcal{F}_L^\dagger \mathcal{H}_L \mathcal{F}_L, \tag{26}$$

where $\mathcal{F}_L$ is a vector of dimension $L+2$,

$$\mathcal{F}_L^\dagger = \left[c_d^\dagger f_0^\dagger f_1^\dagger \cdots f_L^\dagger\right], \tag{27}$$

and $\mathcal{H}_L$ is a $(L+2)\times(L+2)$ matrix whose nonvanishing elements are

$$[\mathcal{H}_L]_{11} = \epsilon_d/D_L, \tag{28}$$

$$[\mathcal{H}_L]_{12} = [\mathcal{H}_L]_{21} = \sqrt{2}V/D_L, \tag{29}$$

and

$$[\mathcal{H}_L]_{n,n+1} = [\mathcal{H}_L]_{n+1,n} = \epsilon_{n-2}/D_L. \tag{30}$$

To diagonalize the Hamiltonian H_L one has to diagonalize the matrix $\mathcal{H}_L$. The pattern followed by the numerical results of this operation has been detailed elsewhere[10]. To summarize, we recall here only that for large, odd L, out of the $L+2$ eigenvalues of $\mathcal{H}_L$, $(L+1)/2$ are always positive, $(L+1)/2$ are always negative, and the remaining eigenvalue has the sign of ϵ_d (it is zero for $\epsilon_d = 0$). For definiteness, we henceforth consider $\epsilon_d \leq 0$, which makes it convenient to denote the positive eigenvalues $\eta_{\ell+}$, with $\ell = 1,\ldots,(L+1)/2$ and the negative ones $-\eta_{\ell-}$, with $\ell = 0,\ldots,(L-1)/2$. To a good approximation, then[10]

$$\eta_{\ell\pm} \approx \Lambda^{\ell - z \mp \gamma_{\ell\pm}}, \tag{31}$$

the $\gamma_{\ell\pm}$ being in turn related to the η_ℓ by

$$\tan(\pi\gamma_{\ell\pm}) = \frac{\Gamma/A_\Lambda}{\epsilon_d \mp D_L\eta_{\ell\pm}}. \tag{32}$$

Here, $\Gamma = \pi V^2/D$ is the impurity level width, $\ell+$ $(\ell-)$ ranges from unity to $(L+1)/2$ $[(L+3)/2]$, and $A_\Lambda = \ln\sqrt{\Lambda}/\tanh(\ln\sqrt{\Lambda})$ converges rapidly to unity as $\Lambda \to 1$.

When Eq. (32) is compared to the exact expression for the phase shifts δ in the uncorrelated Anderson Hamiltonian,

$$\tan\delta = \frac{\Gamma}{\epsilon_d - \epsilon}, \tag{33}$$

we see that the exponents γ_ℓ are discretized versions of the phase shifts divided by π, that is, $\mp\gamma_{\ell\pm} \equiv \delta/\pi$.

V. THERMODYNAMICAL AVERAGES

To compute thermodynamical averages for an impurity Hamiltonian, one must first diagonalize it. In the renormalization-group method, this generally calls for the iterative numerical procedure extensively discussed in previous publications.[1,6,7] For the single-particle Hamiltonian (26), however, the straightforward diagonalization conducted in Sec. IV suffices. For odd L, for instance, a simple calculation[6] shows that, at temperature T, the magnetic susceptibility of the $U=0$ truncated Anderson Hamiltonian H_L is

$$\chi = \frac{(g\mu_B)^2}{2k_BT}\left[\sum_{\ell=1}^{(L+1)/2}\frac{e^{-\bar\beta\eta_{\ell+}}}{(1+e^{-\bar\beta\eta_{\ell+}})^2} + \sum_{\ell=0}^{(L+1)/2}\frac{e^{-\bar\beta\eta_{\ell-}}}{(1+e^{-\bar\beta\eta_{\ell-}})^2}\right]. \tag{34}$$

To compute the impurity contribution $\chi_{\rm imp}$ to the susceptibility, one must subtract from χ the (Pauli) susceptibility of the free electron gas. To this end, one must diagonalize the discretized conduction-band Hamiltonian, which in analogy with Eq. (25), is given by

$$H_{cb}^L = \left[\sum_{n=0}^{L-1}\epsilon_n^z(f_n^\dagger f_{n+1} + \text{H.c.})\right]\Big/ D_L. \tag{35}$$

Also quadratic, this Hamiltonian can be diagonalized by the numerical procedure in Sec. IV. For large, odd L, a symmetric set of $L+1$ eigenvalues $\pm\eta_\ell^*$ $(\ell = 1,\ldots,(L+1)/2)$ results, each of which is approximately given by

$$\eta_\ell = \Lambda^{\ell - z}. \tag{36}$$

Once the eigenvalues of the discretized conduction-band Hamiltonian have been determined, the Pauli susceptibility is easily computed. For odd L, it is given by

$$\chi_{cb} = \frac{(g\mu_B)^2}{k_BT}\sum_{\ell=1}^{(L+1)/2}\frac{e^{-\bar\beta\eta_\ell}}{(1+e^{-\bar\beta\eta_\ell})^2}. \tag{37}$$

The impurity contribution to the susceptibility is

$$\chi_{\rm imp} = \chi - \chi_{cb}. \tag{38}$$

From Eq. (34), it then follows that

$$\chi_{\rm imp}(z,T) = \frac{(g\mu_B)^2}{2k_BT}\left[\frac{e^{-\beta\eta_{0-}}}{(1+e^{-\bar\beta\eta_{0-}})^2} + \sum_{\ell=1}^{(L+1)/2}\Phi(\ell)\right], \tag{39}$$

where we have separated the $\ell = 0$ term from the second sum on the right-hand side of Eq. (34), and

$$\Phi(\ell) = \frac{e^{-\bar\beta\eta_{\ell+}}}{(1+e^{-\bar\beta\eta_{\ell+}})^2} + \frac{e^{-\bar\beta\eta_{\ell-}}}{(1+e^{-\bar\beta\eta_{\ell-}})^2} - 2\frac{e^{-\bar\beta\eta_\ell}}{(1+e^{-\bar\beta\eta_\ell})^2}. \tag{40}$$

The summand on the right-hand side of Eq. (40) becomes very small for ℓ such that $\bar\beta\Lambda^\ell \gg 1$. For sufficiently large L, therefore, it is safe to extend the upper limit of that sum to infinity.

It is also safe to extend the lower limit to $-\infty$. To see this, recall that $\bar\beta$ is small and that the eigenvalues $\eta_{\ell+}$ are of the order of Λ^ℓ, so that for small ℓ the exponential $\exp(-\bar\beta\eta_{\ell+})$ is approximately equal to unity, and the first term on the right-hand side of Eq. (40) is approximately

1/4; the second term is likewise approximately 1/4, while the last one is approximately $-1/2$. The summand thus becomes very small for small ℓ, and we substitute $-\infty$ for 1 in the lower limit of the sum on the right-hand side of Eq. (39), which then becomes

$$\chi_{\rm imp}(z,T) = \frac{(g\mu_B)^2}{2k_BT}\left[\frac{e^{-\bar{\beta}\eta_{0-}}}{(1+e^{-\bar{\beta}\eta_{0-}})^2} + \sum_{\ell=-\infty}^{\infty}\Phi(\ell)\right]. \tag{41}$$

Considered as a function of a complex variable ξ, the summand $\Phi(\xi)$ is real and analytic on the real axis, $\xi = x$. Under these conditions, a Sommerfeld-Watson transformation[17] converts the infinite sum in Eq. (41) into an integral:

$$\sum_{\ell=-\infty}^{\infty}\Phi(\ell) = \int_{-\infty}^{\infty}\Phi(x)\,dx + 4\pi\Im\left(\sum_k{}'R(k)\right), \tag{42}$$

where $R(k)$ indicates the residue of the function

$$\varphi(\xi) = \frac{\Phi(\xi)}{1-\exp(-2\pi i\xi)} \tag{43}$$

at the pole $\xi = \xi_k$. The prime in the last term on the right-hand side of Eq. (42) indicates that the sum runs over all poles in the upper half-plane, $\Im(\xi_k) > 0$.

Since the denominator on the right-hand side of Eq. (43) does not vanish in that half-plane, the (double) poles coincide with those of $\Phi(\xi)$ and are given by

$$1+\exp(-\bar{\beta}\Lambda^{\xi_k - z}) = 0 \tag{44}$$

and

$$1+\exp(-\bar{\beta}\Lambda^{\xi_k - z \mp \gamma_{\xi_k\pm}}) = 0, \tag{45}$$

where the $\gamma_{\xi_k\pm}$ are given by Eq. (32) with the replacement $\eta_\ell \to \xi_k$.

It is easy to show that the poles of $\Phi(\xi)$ lie at or above the line $\Im(\xi) = \pi/(2\ln\Lambda)$. Equation (43) then shows that the largest contributions to $\varphi(\xi_k)$ are proportional to $\exp(-\pi^2/\ln\Lambda)$. Each residue $R(k)$ is therefore proportional to that factor, and for small Λ the sum on the right-hand side of Eq. (42) is negligible. For small Λ, therefore, the infinite sum on the right-hand side of Eq. (41) turns into an integral, showing that the impurity susceptibility calculated with the discretized conduction band is close to the continuum limit.

In order to substantiate this point with a more specific discussion, and to show that for large Λ the second term on the right-hand side of Eq. (42) introduces oscillations in the temperature dependence of the susceptibility, we will now calculate $T\chi_{\rm imp}(z,T)$ at the low-temperature limit. To take the simplest illustration, we consider the impurity at the Fermi energy $\epsilon_d = 0$.

As $T \to 0$, Eq. (17) shows that the truncation limit L approaches infinity. According to Eq. (19), the scaled bandwidth D_L then approaches zero, and according to Eq. (32), $\tan(\pi\gamma_{\ell\pm}) \to \mp\infty$. In this limit, therefore, $\gamma_{\ell\pm} \to \mp 1/2$, so that the eigenvalues in Eq. (31) become

$$\eta_{\ell\pm} = \Lambda^{\ell - z + 1/2}. \tag{46}$$

The function $\Phi(\xi)$ in Eq. (40) then reduces to

$$\Phi(\xi) = 2\left\{\frac{\exp(-\bar{\beta}\Lambda^{\xi-z+1/2})}{[1+\exp(-\bar{\beta}\Lambda^{\xi-z+1/2})]^2} - \frac{\exp(-\bar{\beta}\Lambda^{\xi-z})}{[1+\exp(-\bar{\beta}\Lambda^{\xi-z})]^2}\right\}. \tag{47}$$

In the upper $[\Im(\xi) > 0]$ half-plane, the right-hand side has double poles at $\xi = \xi_k$ and $\xi = \xi_k'$ $(k = 0, 1, \ldots)$ given by

$$\bar{\beta}\Lambda^{\xi_k - z + 1/2} = i\pi(2k+1) \tag{48}$$

and

$$\bar{\beta}\Lambda^{\xi_k' - z} = i\pi(2k+1), \tag{49}$$

respectively. It follows that

$$\xi_k = z - \frac{1}{2} + \frac{(4j+1)i\pi}{2\ln\Lambda} + \frac{\ln[(2k+1)\pi]}{\bar{\beta}\ln\Lambda} \tag{50}$$

and

$$\xi_k' = z + \frac{(4j+1)i\pi}{2\ln\Lambda} + \frac{\ln[(2k+1)\pi]}{\bar{\beta}\ln\Lambda}, \tag{51}$$

where j is any non-negative integer.

Given the denominator $1-\exp(-2\pi i\xi_k)$ on the right-hand side of Eq. (43), the function $\varphi(\xi)$ decreases rapidly with increasing $\Im(\xi)$. The leading contributions to the sum over $R(k)$ on the right-hand side of Eq. (42) therefore come from the poles with $j = 0$ on the right-hand sides of Eqs. (50) and (51). Their residues are

$$R(k) = \frac{2(k+1)}{\pi^2(2k+1)^2}e^{-\pi^2/\ln\Lambda}\exp\left[2\pi i\left(z - 1/2 + \frac{\ln[2\pi(2k+1)]}{\ln\Lambda} + \frac{\ln(k_BT/D_N)}{\ln\Lambda}\right)\right], \tag{52}$$

so that Eq. (42) becomes

$$\sum_{\ell=-\infty}^{\infty}\Phi(\ell) = \int_{-\infty}^{\infty}\Phi(x)\,dx + \frac{8}{\pi}e^{-\pi^2/\ln\Lambda}\sum_{k=0}^{\infty}\frac{(k+1)}{(2k+1)^2}\cos\left[2\pi\left(z - 1/2 + \frac{\ln[2\pi(2k+1)]}{\ln\Lambda} + \frac{\ln(k_BT/D_N)}{\ln\Lambda}\right)\right], \tag{53}$$

and Eq. (41) becomes

$$\chi_{\rm imp}(z,T)=\frac{(g\mu_B)^2}{2k_BT}\left\{\frac{e^{-\beta\eta_{0-}}}{(1+e^{-\beta\eta_{0-}})^2}+\int_{-\infty}^{\infty}\Phi(x)\,dx\right.$$
$$\left.+\frac{8}{\pi}e^{-\pi^2/\ln\Lambda}\sum_{k=0}^{\infty}\frac{(k+1)}{(2k+1)^2}\cos\left[2\pi\left(z-1/2+\frac{\ln[2\pi(2k+1)]}{\ln\Lambda}+\frac{\ln(k_BT/D_N)}{\ln\Lambda}\right)\right]\right\}. \quad (54)$$

For impurity energy $\epsilon_d=0$, the eigenvalue η_{0-} is zero for all L and the first term within curls on the right-hand side of Eq. (54) is 1/4. The integral in the second term, on the other hand, equals[18] $-1/4$, so that the two terms add up to zero. We are left with

$$\chi_{\rm imp}=\frac{(g\mu_B)^2}{k_BT}\frac{4}{\pi}e^{-\pi^2/\ln\Lambda}\left\{\sum_{k=0}^{\infty}\frac{(k+1)}{(2k+1)^2}\cos\left[2\pi\left(z-1/2+\frac{\ln[2\pi(2k+1)]}{\ln\Lambda}+\frac{\ln(k_BT/D_N)}{\ln\Lambda}\right)\right]\right\}. \quad (55)$$

This expression illustrates the central points raised in this paper. In the low-temperature limit, one expects the impurity contribution to the susceptibility to vanish. The entire right-hand side must therefore be an artifact of the logarithmic discretization of the conduction band, and indeed the exponential function multiplying the curly brackets guarantees that it vanish for $\Lambda\to 1$. For small Λ, the deviation is minute; that exponential function guarantees rapid convergence (as a function of Λ) to the continuum limit $T\chi_{\rm imp}=0$.

For increasing Λ, however, by the time the discretization parameter becomes comparable to 10, the right-hand side of Eq. (55) has ceased to be negligible. The logarithmic temperature dependence within the argument of the cosine makes $T\chi_{\rm imp}(T)$ oscillate with period $\ln\Lambda$. Such behavior is visible in every calculation of a thermodynamical average, as illustrated by Fig. 1. The amplitude of the oscillations depends on the model Hamiltonian, the calculated property, and on the temperatures at which it is computed.

Inspection of Eq. (55) shows also that the phase of the oscillations is a linear function of the sliding parameter z. By averaging the calculated susceptibility over z we eliminate the deviations from the continuum limit; i.e., we recover the result $T\chi_{\rm imp}\to 0$, exact at low temperatures.

At higher temperatures, the energy dependence of the phase shifts γ [see Eq. (32)] makes the analysis of Eq. (41) cumbersome. We prefer to discuss the numerical results in Figs. 3 and 4.

The solid circles in those figures show that the deviations on the right-hand side of Eq. (55) are not restricted to the low-temperature regime. The impurity susceptibility calculated with a fixed sliding parameter z and large Λ oscillates as a function of temperature; plotted on a logarithmic scale the oscillations have period $\ln\Lambda$. By contrast, since the amplitudes of the oscillations grow in proportion to $\exp(-\pi^2/\ln\Lambda)$, calculations carried out with $1<\Lambda\le 3$ are satisfactorily accurate, as the inset in Fig. 4 shows.

The derivation of Eq. (55) indicates that the sinusoidal deviations are mathematical analogs of the de Haas–van Alphen oscillations. The latter are due to the physical bunching of conduction band states due to an external magnetic field; the former are due to the logarithmic discretization of the conduction band. One therefore expects them to disappear when the physical properties calculated as functions of the discretization parameter z are integrated from $z=0$ to $z=1$, since the discrete levels in Fig. 2 then run over the entire conduction band.

The integration must be carried out numerically. To consider the crudest approximation, one that nevertheless ensures rapid convergence to the continuum limit, we employ a two-point trapezoidal rule. Thus, instead of computing the susceptibility for fixed sliding z as illustrated by the solid circles in Figs. 3 and 4, we calculate the z-integrated susceptibility $\chi_{\rm imp}(T)=\int_0^1\chi_{\rm imp}(z,T)\,dz$ with the approximate expression

$$\chi_{\rm imp}(T)=\chi_{\rm imp}(z=0.25,T)(0.5-0)$$
$$+\chi_{\rm imp}(z=0.75,T)(1-0.5) \quad (56)$$

or, which is the same,

$$\chi_{\rm imp}(T)=[\chi_{\rm imp}(0.25,T)+\chi_{\rm imp}(0.75,T)]/2\,. \quad (57)$$

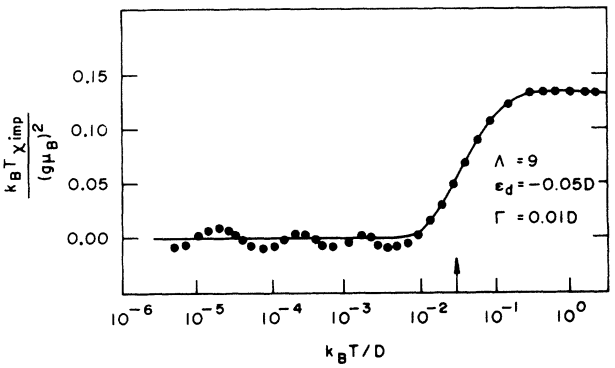

FIG. 3. Temperature dependence of the impurity susceptibility calculated with discretization parameter $\Lambda=9$ for impurity energy $\epsilon_d=-0.05\,D$, larger in absolute value than the level width $\Gamma=0.01\,D$. The solid circles represent results obtained with the standard procedure (Refs. 1 and 6). The solid line is the susceptibility computed with the interleaved procedure. The vertical arrow on the horizontal axis indicates the crossover temperature $k_BT=\epsilon_d$, which separates the free-impurity regime $[k_BT\chi_{\rm imp}/(g\mu_B)^2=1/8]$ from the frozen-impurity regime $[k_BT\chi_{\rm imp}/(g\mu_B)^2=0]$. In the latter, the discretization of the conduction band introduces oscillations with period $\ln\Lambda$ in the curve represented by the solid circles. By contrast, the interleaved procedure yields results indistinguishable on the scale of the plot from the exact curves for the impurity susceptibility.

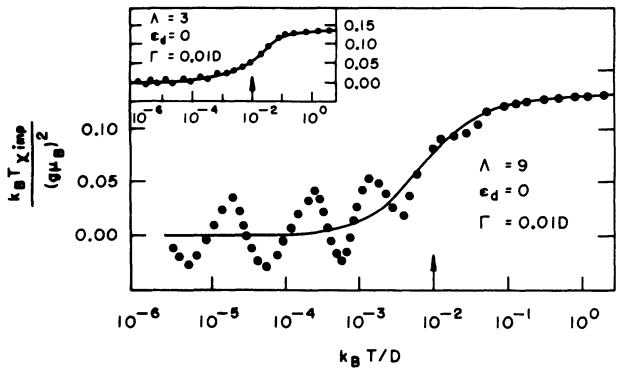

FIG. 4. Temperature dependence of the impurity susceptibility calculated with discretization parameter $\Lambda = 9$ for impurity energy $\epsilon_d = 0$ and level width $\Gamma = 0.01\,D$. The vertical arrow along the horizontal axis indicates the crossover temperature $k_B T = \Gamma$ from the free-impurity to the frozen-impurity regime. As in Fig. 3, the solid circles represent susceptibilities obtained with the standard procedure (Refs. 1 and 6), while the solid line shows the susceptibility calculated with the interleaved procedure. The large difference between the conduction-band phase shifts in the interacting system in the frozen-impurity regime and those in the free-electron gas from which the Pauli susceptibility is calculated makes the oscillations in the curve represented by the solid circles particularly large; the inset, calculated with $\Lambda = 3$, shows that such oscillations increase rapidly with growing Λ, thus rendering the computation of thermodynamical averages with $\Lambda > 3$ impossible with the standard method. By contrast, the results of the interleaved procedure are remarkably independent of the discretization parameter.

Notice that the two sliding parameters $z = 0.25$ and $z = 0.75$ on the right-hand side correspond to interleaved intervals in the logarithmic discretization depicted in Fig. 2; from this image derives the name we have given to the procedure.

The results of this procedure are shown by the solid lines in Figs. 3 and 4. Even with this simple approximation, the integration washes out the oscillations and yields a curve for the temperature-dependent susceptibility that cannot be distinguished from the continuum limit[19–21] on the scale of the plot.

Before closing this section, we comment on the scope of the interleaved procedure. The rapid convergence to the continuum is no special property of the $U = 0$ model. For nonzero U, under the renormalization-group transformation (21), in certain temperature ranges (at low temperatures, for instance) the Anderson Hamiltonian flows to the vicinity of single-particle fixed-point Hamiltonians.[6] To such Hamiltonians, and therefore to such ranges, the analysis in Eqs. (39–55) applies; it follows that integration over the sliding parameter z will eliminate the artificial oscillations introduced by the discretization. In the remaining (crossover) section(s) of the temperature axis, one has to rely on results such as those for the Kondo Hamiltonian (i.e., the $U \to \infty$ limit of the spin-degenerate Anderson Hamiltonian) in Fig. 1. As illustrated by that figure, the numerically computed temperature dependence of the impurity susceptibility shows that in the crossover region(s) the procedure ensures equally rapid convergence to the $\Lambda \to 1$ limit.

The accuracy of the interleaved procedure is therefore independent of U. This, in fact, could be expected: Similar to the standard method, the new approach involves approximations affecting only the conduction Hamiltonian; consequently, it is uniformly accurate over the parametrical space of the model.

VI. CONCLUSIONS

Earlier publications have shown that the sliding parameter z, introduced by the generalized discretization in Fig. 2, extends the scope of the numerical renormalization-group method to encompass the computation of excitation properties.[10–13] As a matter of practical interest, the most recent of those applications have shown that accurate results, quantitatively representative of the continuum limit, are obtained even with discretization parameters Λ as large as 12. In this work, we have shown that, with the interleaved procedure afforded by the generalized, z-dependent discretization, thermodynamical properties calculated with equally large Λ's also yield remarkably accurate averages.

By greatly reducing the computational cost of diagonalizing many-body Hamiltonians, this development aids the analysis of impurity Hamiltonians involving more degrees of freedom than the thoroughly studied single-impurity Anderson model. As an application of this procedure, the magnetic susceptibility for the two-impurity spin-degenerate Kondo Hamiltonian is currently under study[22] with discretization parameter $\Lambda = 10$. Preliminary results show that the model Hamiltonian can be diagonalized with small computational cost and the estimated absolute error for the product $k_B T \chi_{\rm imp}(T)/(g\mu_B)^2$ at any given temperature lies below 5×10^{-3}.

ACKNOWLEDGMENTS

This work has been supported by fellowships from the Coordination for the Improvement of Higher Education (CAPES) and by a grant from the Council for Scientific and Technological Development (CNPq).

* On leave from the Universidade Federal Fluminense, Niterói, RJ, Brazil.

[1] K. G. Wilson, Rev. Mod. Phys. **47**, 773 (1975).
[2] H. R. Krishna-murthy, K. G. Wilson, and J. W. Wilkins, Phys. Rev. Lett. **35**, 1101 (1975).
[3] B. A. Jones and C. M. Varma, Phys. Rev. Lett. **58**, 843 (1987).
[4] B. A. Jones, C. M. Varma, and J. W. Wilkins, Phys. Rev. Lett. **61**, 125 (1988).
[5] B. A. Jones and C. M. Varma, Phys. Rev. B **40**, 324 (1989).

[6] H. R. Krishna-murthy, J. W. Wilkins, and K. G. Wilson, Phys. Rev. B **21**, 1003 (1980).
[7] H. R. Krishna-murthy, J. W. Wilkins, and K. G. Wilson, Phys. Rev. B **21**, 1044 (1980).
[8] L. N. Oliveira and J. W. Wilkins, Phys. Rev. Lett. **47**, 1553 (1981).
[9] B. Alascio, R. Allub, and C. A. Balseiro, Phys. Rev. B **34**, 4786 (1986).
[10] M. Yoshida, M. A. Whitaker, and L. N. Oliveira, Phys. Rev. B **41**, 9403 (1990).
[11] H. O. Frota and L. N. Oliveira, Phys. Rev. B **33**, 7871 (1986).
[12] V. L. Líbero and L. N. Oliveira, Phys. Rev. Lett. **65**, 2042 (1990).
[13] V. L. Líbero and L. N. Oliveira, Phys. Rev. B **42**, 3167 (1990).
[14] A. M. Tsvelick and P. B. Wiegmann, Adv. Phys. **32**, 453 (1983).
[15] L. N. Oliveira, Braz. J. Phys. **22**, 155 (1992).
[16] See, e.g., R. Haydock, in *Solid State Physics*, edited by H. Ehrenreich, F. Seitz, and D. Turnbull (Academic, New York, 1980), Vol. 35, p. 215.
[17] J. Mathews and R. L. Walker, *Mathematical Methods of Physics*, 2nd ed. (Benjamin, Menlo Park, CA, 1970), p. 75.
[18] I. S. Gradshteyn and I. M. Ryzhik, *Tables of Integrals, Series, and Products* (Academic, New York, 1965), p. 352, Eq. 3.527.3.
[19] N. Rivier and M. J. Zuckermann, Phys. Rev. Lett. **21**, 904 (1968).
[20] K. D. Schotte and U. Schotte, Phys. Lett. **55A**, 38 (1975).
[21] M. Salomaa, Z. Phys. B **25**, 49 (1976).
[22] J. B. Silva, W. C. Oliveira, J. L. N. Mello, and L. N. Oliveira (unpublished).